Mechanical signaling coordinates the embryonic heartbeat

Kevin K. Chiou[a], Jason W. Rocks[a], Christina Yingxian Chen[b], Sangkyun Cho[c], Koen E. Merkus[d], Anjali Rajaratnam[b], Patrick Robison[c], Manorama Tewari[c], Kenneth Vogel[c], Stephanie F. Majkut[c], Benjamin L. Prosser[b], Dennis E. Discher[c], and Andrea J. Liu[a,1]

[a]Department of Physics and Astronomy, University of Pennsylvania, Philadelphia, PA 19104; [b]Department of Physiology, Pennsylvania Muscle Institute, University of Pennsylvania Perelman School of Medicine, Philadelphia, PA 19104; [c]Molecular and Cell Biophysics Laboratory, University of Pennsylvania, Philadelphia, PA 19104; and [d]Applied Physics, Eindhoven University of Technology, 5600 MB Eindhoven, The Netherlands

Edited by David A. Weitz, Harvard University, Cambridge, MA, and approved June 14, 2016 (received for review October 16, 2015)

In the beating heart, cardiac myocytes (CMs) contract in a coordinated fashion, generating contractile wave fronts that propagate through the heart with each beat. Coordinating this wave front requires fast and robust signaling mechanisms between CMs. The primary signaling mechanism has long been identified as electrical: gap junctions conduct ions between CMs, triggering membrane depolarization, intracellular calcium release, and actomyosin contraction. In contrast, we propose here that, in the early embryonic heart tube, the signaling mechanism coordinating beats is mechanical rather than electrical. We present a simple biophysical model in which CMs are mechanically excitable inclusions embedded within the extracellular matrix (ECM), modeled as an elastic-fluid biphasic material. Our model predicts strong stiffness dependence in both the heartbeat velocity and strain in isolated hearts, as well as the strain for a hydrogel-cultured CM, in quantitative agreement with recent experiments. We challenge our model with experiments disrupting electrical conduction by perfusing intact adult and embryonic hearts with a gap junction blocker, β-glycyrrhetinic acid (BGA). We find this treatment causes rapid failure in adult hearts but not embryonic hearts—consistent with our hypothesis. Last, our model predicts a minimum matrix stiffness necessary to propagate a mechanically coordinated wave front. The predicted value is in accord with our stiffness measurements at the onset of beating, suggesting that mechanical signaling may initiate the very first heartbeats.

mechanotransduction | excitable media | cardiac development | heartbeat | reaction–diffusion

The heart is a prime example of an active system with mechanical behavior—the heartbeat—that is robust and remarkably well coordinated. The fundamental contractile units of the heart are muscle cells called cardiac myocytes (CMs). Individual CMs coordinate their contractions through intercellular signaling, generating contractile wave fronts that propagate through the tissue to pump macroscopic volumes of fluid. When this organization breaks down, tissue-scale contractions cease and blood circulation stops. It has long been understood that this signal is electrical (1): ions pass from one cell to another through gap junctions (2), depolarizing the cell membrane and initiating a process that ultimately releases Ca^{2+} from intracellular stores, driving CM contraction. The potential difference between CMs drives ion transport through gap junctions into the next cell, thus propagating the signal. This electrical signaling cascade is responsible for the contractile wave fronts of the heartbeat in adults and has been assumed to regulate the heartbeat at all stages of development. Here, we propose that the early embryonic heart does not follow this established electrical signaling mechanism, but may instead use mechanical signaling to coordinate and propagate its beat. In our picture, embryonic CMs are mechanically excitable: we postulate that sufficiently high strains trigger intracellular release of Ca^{2+} ions through a molecular mechanism that is not yet determined, leading to contraction. We denote this mechanically driven release of Ca^{2+} ions and subsequent contraction as mechanical activation. This in turn strains neighboring CMs and induces additional contraction, resulting in a coordinating signal that is propagated mechanically rather than electrically.

Although embryonic CMs beat spontaneously (3, 4), they would contract with random phases in the absence of a coordinating signal. A number of studies have shown that embryonic, neonatal, and adult CMs are sensitive to mechanical cues (5–9). Recently, the role of mechanics was explored at the tissue scale through extracellular matrix (ECM) stiffening and softening of isolated avian embryonic hearts (10). The speed and strain of the contractile wave front were found to be strongly dependent upon the tissue stiffness, suggesting that the electrical signaling picture is insufficient for the embryonic heart and that the stiffness of the matrix must be taken into account.

Here, we show that mechanical signaling between CMs can explain stiffness-dependent contractile wave front speed and strain via a nonlinear mechanical "reaction–diffusion" mechanism, in which sufficient strain on a CM causes it to "react" by triggering contraction and stress "diffuses" through the tissue. Few models of CM signaling in the heart include mechanics; of these, most assume instantaneous mechanical signal propagation (11, 12) and therefore do not exhibit strong stiffness dependence. Our model is related to a mechanical version (10, 13) of the fire–diffuse–fire model (14), which also fails to capture key stiffness-dependent features. We model the heart as tissue composed of active and

Significance

There is a mounting body of evidence that physical forces induce biochemical changes. Here, we suggest that the early embryonic heart provides a striking illustration of the importance of mechanics in living matter. Whereas adult hearts use electrical signaling to coordinate the heartbeat, we propose that embryonic hearts use mechanical signaling. We model the embryonic heart as mechanically excitable tissue, with cardiac myocytes that are triggered to contract under strain. Such contractions exert strains on nearby cells and induce further contraction, thus propagating the signal through the heart. This simple model captures key features observed in the heartbeat of stiffness-modified embryonic hearts that cannot be explained by standard electrochemical signaling and yields predictions that we confirm with experiments.

Author contributions: K.K.C., S.F.M., B.L.P., D.E.D., and A.J.L. designed research; K.K.C., J.W.R., C.Y.C., S.C., K.E.M., A.R., P.R., M.T., and K.V. performed research; K.K.C., J.W.R., C.Y.C., S.C., K.E.M., P.R., and M.T. contributed new reagents/analytic tools; K.K.C., C.Y.C., S.C., K.E.M., and A.R. analyzed data; K.K.C. and J.W.R. performed numerical calculations; and K.K.C., B.L.P., D.E.D., and A.J.L. wrote the paper.

Conflict of interest statement: K.K.C. is a former PhD student of PNAS Editorial Board member Boris I. Shraiman.

This article is a PNAS Direct Submission.

[1]To whom correspondence should be addressed. Email: ajliu@physics.upenn.edu.

This article contains supporting information online at www.pnas.org/lookup/suppl/doi:10.1073/pnas.1520428113/-/DCSupplemental.

passive components. We treat the active CMs as mechanically excitable inclusions that contract when the local strain exceeds a threshold value. The surrounding ECM is treated as a passive elastic-fluid biphasic material. This simple mechanical signaling model quantitatively captures the stiffness dependence of contractile wave front velocity and strain, as well as the strain of CMs cultured on hydrogels observed in ref. 10.

We challenge the hypothesis underlying our model—that mechanical signaling coordinates the embryonic heart—by blocking gap junctions with 18-β-glycyrrhetinic acid (BGA). We find that embryonic hearts continue to beat, even at BGA concentrations 10-fold higher than those sufficient to stop the adult heartbeat in minutes, confirming our hypothesis. Finally, our model predicts a minimum matrix modulus necessary to support a steady-state mechanical wave front. We show experimentally that this value is consistent with the heart's stiffness when it first starts to beat. Thus, the heart, the first functional organ in the embryo, begins to beat as soon as mechanical signaling can support propagating wave fronts.

Production of CMs from pluripotent stem cells has generated considerable interest in the factors that govern maturation of these cells to heart tissue (15) particularly for repair of adult heart damage. Mechanical determinants in this process remain poorly understood, although the role of mechanical cues is increasingly recognized in cell differentiation, proliferation, and morphogenesis (16–19). Our results here indicate that mechanics in the developing heart may be necessary to tissue-scale function during stem cell maturation and may have application to heart damage repair.

Physical Model of Cardiac Mechanical Signaling

The myocardium of the embryonic heart is composed primarily of mechanically excitable CMs (that contract when activated) and the surrounding ECM. We treat CMs as elastic inclusions embedded in the ECM, in accord with recent experiments of CMs embedded in 3D hydrogels (20). We ignore direct cell–cell mechanical coupling; experimental evidence indicates that stresses are transmitted primarily through cell–matrix adhesions rather than cell–cell contacts during development (21), likely due to the prevalence of cell–junction remodeling. In addition, collagenase treatment indicates that ECM is the primary component of tissue structural integrity (10). We find that a good approximation (*Materials and Methods*) is to consider CMs as infinitesimal and arranged in a cubic array, spaced by $\Delta x = 10$ μm (Table 1). We consider a 3D mechanical version of fire-diffuse-fire signaling. This requires capturing the physics of (*i*) activated CMs creating mechanical stress; (*ii*) stress propagation between CMs; and (*iii*) activation of quiescent CMs in response to mechanical stress in the ECM.

Table 1. Parameter symbols, references, and values

Parameter	Symbol	Value (fit/ref.)
Mesh/fluid drag	Γ	0.4 mPa·s/μm^2 (Fit)
E4 myocardium modulus	E^*	1.6 kPa (10)
ECM Poisson ratio	ν	0.4 (26)
Fluid fraction (average)	ϕ	0.8 (50, 51)
Fluid viscosity (water, 25 °C)	η	0.89 mPa·s
CM spacing	Δx	10 μm (10)
CM modulus	E^c	0.75 kPa (fit)
CM eigenstrain magnitude	ϵ^*	0.2 (6)
CM strain threshold	α	0.11 (fit)
CM Poisson ratio	ν^c	0.4 (26)
Contraction time (AP duration)	τ	250 ms

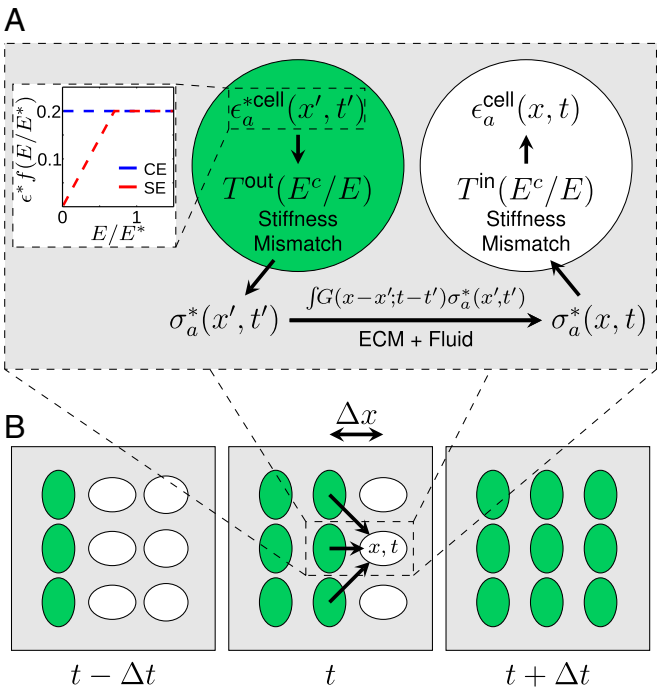

Fig. 1. Model for stress propagation in the myocardium. (*A*, *Inset*) CE and SE models as a function of ECM Young's modulus, which determines the strength of contraction (Eq. **1**). (Main) The contracting CM (green) acts as a stress source for a quiescent CM (white). An activated cell *a* contracts with an eigenstrain $\epsilon^{*\text{cell}}_{a,ij}(x',t')$, locally inducing a stress $\sigma^*_{a,ij}(x',t')$ in the ECM that depends on the relative stiffness between the ECM and CMs. We capture these physics via the tensor T^{out}_{ijkl} in accordance with the Eshelby theory of elastic inclusions (*Supporting Information*). This stress propagates according to the ECM response function $G_{ijkl}(x-x',t-t')$ (*Supporting Information*). The matrix stress at (x,t) due to cell *a* is $\sigma_{a,ij}(x,t)=\int d^3x'dt'G_{ijkl}(x-x',t-t')\sigma^*_{a,kl}(x',t')$. This creates $\epsilon^{\text{cell}}_{a,ij}(x,t)$, the strain induced in the quiescent CM due to the contraction of *a* (modified by T^{in}_{ijkl}). (*B*) Sketch depicting quiescent (white) and activated (green) CMs in a traveling mechanical wave front at subsequent activation times separated by Δt. Arrows represent stresses propagated through the ECM (not all shown) to a quiescent CM, which activates when $\epsilon^{\text{cell}}_{ii}(x,t)\geq\alpha$.

How Activated CMs Create Stress. We use two models to characterize the eigenstrain, i.e., the strain of an active inclusion (CM) in the absence of external stresses. In the constant eigenstrain (CE) model, we assume that CMs contract with a fixed eigenstrain independent of ECM stiffness. In the saturating eigenstrain (SE) model, the eigenstrain increases linearly with Young's modulus E up to a stall stiffness E_s, and is independent of E for $E>E_s$ (Fig. 1*A*, *Inset*). This behavior is observed for embryonic and neonatal CMs cultured on hydrogels (5, 7, 8, 22) and has been studied theoretically (23).

The two models for the strain exerted by a CM when it contracts are as follows:

$$\begin{aligned}\epsilon^*_{ij}&=\epsilon^*f(E/E_s)Q_{ij},\\ f_{\text{CE}}(E/E_s)&=1 \qquad \forall E\\ f_{\text{SE}}(E/E_s)&=\begin{cases}E/E_s & E<E_s\\ 1 & E\geq E_s\end{cases},\end{aligned} \qquad [1]$$

where Q_{ij} is the strain tensor representation of a uniaxial contraction in the x direction (*Supporting Information*) and ϵ^* is the magnitude of the eigenstrain in the CE model or of the eigenstrain for $E>E_s$ in the SE model. See Fig. 1*A*, *Inset*.

The eigenstrain ϵ^*_{kl} from the activated CM induces a stress in the matrix. To properly capture the physical effects of differences in stiffness between CMs and their surrounding ECM, we use

Eshelby's theory of elastic inclusions (24, 25). We compute the tensor $T^{\text{out}}_{ijkl}(E)$, which relates the CM eigenstrain to the stress it induces in the ECM, shown schematically in Fig. 1*A* (see *Supporting Information* for detailed calculations). The resulting ECM stress source due to an activated CM takes the following form:

$$\sigma^*_{a,ij}(x,t) = T^{\text{out}}_{ijkl}\epsilon^*_{kl}\Theta(t-t_a)\Theta(\tau+t_a-t)\delta^3(x-x_a), \qquad [2]$$

where $\Theta(t)$ is the Heaviside function.

How Stress Propagates Between CMs. At the cellular length scale and CM contraction velocity scale, the Reynolds number is small ($\sim 10^{-5}$). We therefore model the ECM as an overdamped, incompressible biphasic material. See Table 1 for parameter values. It is composed of a linear elastic mesh [with Young's modulus E and Poisson ratio $\nu = 0.4$ (10, 26)] and interstitial fluid (of viscosity η similar to water). The fluid and elastic components are coupled through incompressibility and a drag term Γ, an effect of matrix permeability to fluid. Similar approaches were used to model collagenous tissue (27) and active gels (28). Using this model, we calculate the response function $G_{ijkl}(x,t)$ to describe propagation of mechanical stress within the ECM (*Supporting Information*).

How Quiescent CMs Are Activated Mechanically. We assume that, when the strain on a quiescent CM exceeds threshold α [$\epsilon^{\text{cell}}_{kk}(x_q,t) \geq \alpha$], the CM is activated (it contracts). To describe this mathematically, we index noncontracting (quiescent) cells with q and contracting (active) cells with a. Each activated CM contracts for a physiologically relevant amount of time τ before deactivating and becoming refractory. We assume that the refractory timescale is longer than mechanical relaxation, allowing us to ignore backpropagation. Let us consider a CM at x_a that activated at time t_a. Then t_a is the moment when this CM's strain trace first crossed the strain activation threshold $\epsilon^{\text{cell}}_{kk}(x_a,t_a) = \alpha$, transforming the originally quiescent CM into an active one. The active CM contracts, creating an eigenstrain ϵ^*_{kl} (Eq. **1**) for time $t_a < t < t_a + \tau$, which can be represented as a product of Heaviside functions.

To relate the strain on an embedded quiescent CM q at (x_q,t) due to local mechanical stress within the ECM, we compute the tensor $T^{\text{in}}_{ijkl}(E)$ (also shown schematically in Fig. 1*A*) using elastic inclusion theory (*Supporting Information*). The strain contribution on q from an activated CM a is then as follows:

$$\epsilon^{\text{cell}}_{a,ij}(x_q,t) = T^{\text{in}}_{ijkl}\int G_{klmn}(x_q - x'; t-t')\sigma^*_{a,mn}(x',t'), \qquad [3]$$

with $\sigma^*_{a,mn}(x',t')$ from Eq. **2**. The total strain induced in q is the sum over the contribution from all activated cells $\epsilon^{\text{cell}}_{ij}(x_q,t) = \sum_a \epsilon^{\text{cell}}_{a,ij}(x_q,t)$.

Results

Mechanical Signaling Model Yields Contractile Wave Fronts. From the model, we calculate the velocity of the propagating contractile wave front as a function of matrix stiffness as follows. When a CM contracts, it creates a stress field $\sigma^*_{a,ij}$ in the ECM that can induce further contraction by activating quiescent CMs. If the activation process cascades through the tissue, the resulting contraction wave front can attain a comoving steady state $\epsilon_{ij}(x,t) = \epsilon_{ij}(x-vt)$ with velocity v. This is unsurprising because the model is a mechanical analog of nonlinear reaction-diffusion; such systems are well known to exhibit propagating wave front solutions. The activation condition $\epsilon^{\text{cell}}_{kk}(x,t) = \alpha$ with a comoving steady state relates the wave front velocity v to the model parameters through an algebraic relation (*Supporting Information*). Once v is determined, we compute the maximal tissue strain by coarse-grained solution of the waveform (*Supporting Information*).

Mechanical Signaling Model Fits Experimental Wave Front Velocities with Physiologically Relevant Parameters. We obtain most of the physiological parameter values from the literature (Table 1). We treat CMs as elastic inclusions with Young's modulus E^c and with the same Poisson ratio as the surrounding tissue (26) and estimate CM eigenstrain magnitude to be $\epsilon^* = 0.2$ from intracellular embryonic CM principal strain measurements (6). Stress saturation stiffness is estimated to be the cell modulus $E_s = E^c$ (5, 6). Three model parameters could not be identified from the literature and are fit via nonlinear regression to wave front velocity data from ref. 10. These three parameters are the mesh-fluid drag Γ, the CM activation threshold α, and the effective CM Young's modulus E^c. All three fit values (Table 1) fall within physiologically sensible ranges. The resulting velocity is plotted against ventricle contraction velocity data (black circles, from ref. 10) of stiffness-modified embryonic day 4 (E4) hearts in Fig. 2*A*. No steady-state solution exists below stiffness E_0 (which differs between CE and SE models). Physically, E_0 arises because when the tissue is too soft, contracting CMs cannot provide enough strain to trigger additional contraction in quiescent CMs. This is consistent with a significantly reduced likelihood of wave front propagation observed in experiment (green triangles in Fig. 2*B*). Likewise, the wave front velocity vanishes at high tissue stiffness, where the stiffness mismatch between CMs and the surrounding ECM prevents contracting CMs from exerting sufficient strain on the ECM to trigger contraction of quiescent cells.

Calculated Wave Front Strain Agrees with Experimental Observations with No Additional Fitting Parameters. Using the three parameters (Γ, α, E^c) fit from wave front velocity data, we independently calculate the tissue strain of the contractile wave front and compare with the measured maximal ventricular strain from ref. 10 (Fig. 2*B*). Both the CE (blue) and SE (red) models are in excellent quantitative agreement with the observed behavior (black circles) as a function of tissue stiffness, providing strong evidence in favor of our model. Note that the correct optimum stiffness naturally emerges from our model by treating CMs as elastic inclusions (*Supporting Information*) embedded within a surrounding matrix of variable stiffness. This quantitative agreement is significant and nontrivial, as we can observe from the different values of E corresponding to optimum velocity and optimum strain in experiment and model. Note also that no purely electrochemical model can correctly predict strain as a function of stiffness.

SE Model Is Consistent with Cell-on-Gel Measurements with No Additional Fitting Parameters. We further test our model by comparing to data for beating E4 CMs cultured on polyacrylamide gel where gel strain at cell edges was measured for varying gel stiffness (10). We calculate the trace of the 2D projected strain by finite-element simulation (*Materials and Methods* and Fig. S1) using the fit E^c value and comparing to experiment in Fig. 2*C*. The failure of the CE model on soft gels is expected from cultured CM experiments (7, 8, 22). Remarkably, we find agreement between the SE model with cell-on-gel measurements, demonstrating that we can deduce this single CM behavior as a function of E quantitatively from collective behavior in tissue.

Mechanical Signaling Model Correctly Predicts Appearance of First Heartbeats. The developing heart stiffens with age due to increased collagen in the ECM (10). CMs begin periodic contractions at about 1.5 d after fertilization (E1.5). At that point, the heart does not beat but "shivers"; this shivering is similar to behavior observed in strain-activated contractile cell aggregates (29), which lack a signaling mechanism to coordinate the phases of the periodically contracting cells. The first fully coordinated beats do not occur until hours after CMs start contracting. Our model predicts that coordinated beats cannot appear until the matrix reaches the

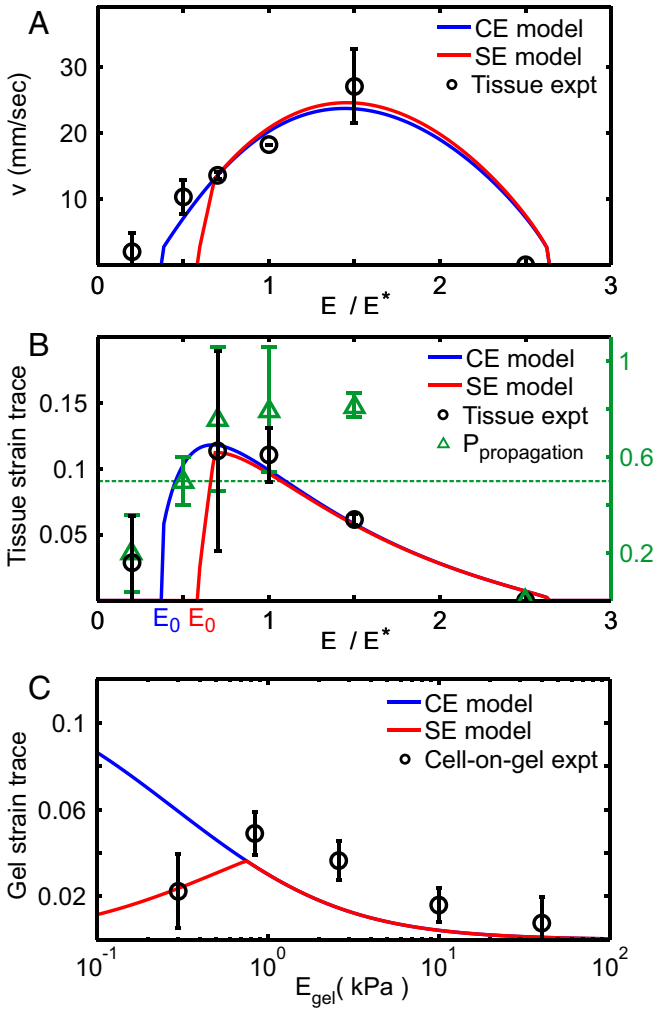

Fig. 2. Results from CE (blue) and SE (red) models (Eq. **1**) compared with experimental measurements (black) from ref. 10. (*A*) Best fits (Table 1) of model contractile wave front velocities to experimental data from the embryonic ventricle. (*B*) Maximal tissue strain as a function of E calculated with no additional fit parameters vs. experimental data (black circles). Green triangles denote likelihood that wave front propagated across the entire ventricle in experiment; for the two lowest E/E^* data points, the likelihood falls below 50% (green dotted line), consistent with our models, which predict no stationary solutions below E_0. (*C*) Predicted induced strain trace for a single cell adhered to gel surface (*Supporting Information*) compared with cell-on-gel data (black circles).

minimum stiffness E_0 (Fig. 2*A*). Here, we ask whether the predicted value of E_0 coincides with heart stiffness at the onset of beating.

We measure embryonic chick hearts stiffnesses at Hamburger–Hamilton (HH) stages 10 and 11 (E1.5–E2) via micropipette aspiration (*Materials and Methods*). Early stage 10 does not exhibit fully coordinated beats, whereas stage 11 exhibits full-tissue contraction (Movie S1). At the strains applied, the tissue behaves as a standard linear solid (Fig. S2).

We sort the measured stiffnesses depending on whether or not the hearts exhibit coordinated contractions (black circles in Fig. 3). The prebeating stiffness is just above that of the undifferentiated embryonic disk (10), suggesting that the first stage of heart development involves some differentiation with little stiffening. The minimum stiffnesses E_0 for the CE (blue) and SE (red) models both fall between the measured prebeating and postbeating values. These measurements are consistent with our model prediction and suggest that heartbeats may initially emerge once the tissue becomes stiff enough to support mechanically activated wave fronts.

Conduction Interference Experiments Are Consistent with Mechanically Coordinated Heartbeats. Gap junctions are critical for electrical coordination of adult heartbeats. Our mechanical signaling hypothesis implies that blocking electrical signaling should not impede the embryonic heartbeat. We therefore test our hypothesis by blocking electrical signaling through pharmacological interference of gap junctions.

We perfuse isolated adult and embryonic hearts with BGA, a nonspecific gap junction blocker known to inhibit intercellular ion transport between embryonic chick epithelial cells at 10 μM (30) and in rat, frog, mouse, and human systems (31–34). Adult hearts stopped beating within 10 min posttreatment at 25 μM BGA (Fig. S3 and Movie S2). However, the embryonic heartbeat was unaffected for 1 h even at 100 μM BGA (Fig. 4), and was robust even when subjected to 250 μM for an additional hour. We also validated its effect in embryonic hearts via fluorescence recovery after photobleaching (FRAP) experiments and found that BGA treatment reduced intercellular diffusion (*Supporting Information*, Fig. S4, and Movie S3). Additionally, our protocol successfully perfuses the embryonic heart with other small-molecule drugs such as blebbistatin and mecarbil (Figs. S5 and S6). These experiments demonstrate that embryonic CMs can coordinate their contractions without functional gap junctions needed to support electrical signaling, supporting our hypothesis of mechanically coordinated CMs in the early heart (*Materials and Methods*).

Discussion

Mechanical Signaling Robustly Explains Strong Dependence of Wave Front Velocity and Strain on Stiffness. Tissue stiffness is a mechanical property that cells can sense. A strong dependence on tissue stiffness is an indicator of cell response to mechanical cues. Our model combines elasticity with simple mechanical activation of CMs, using a minimum of assumptions and adjustable parameters, and yet captures multiple observed cell- and tissue-scale phenomena quantitatively.

Our model is robust to noise: the predicted strain threshold α requires several nearest-neighbor contractions to trigger activation. As a result, a rogue contraction cannot set off a wave front. Our results are also robust to how we incorporate mechanosensitivity. We considered a model variant in which the CM

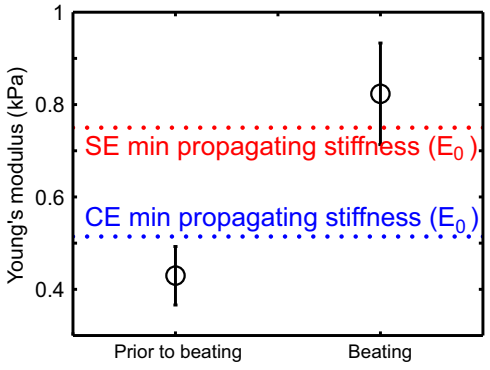

Fig. 3. Measurements of heart stiffness before and after the appearance of heartbeats, compared with minimum stiffness necessary to support a mechanically coordinated contraction in our model. Stiffness is measured via micropipette aspiration for six Hamburger–Hamilton (HH) stage 10 and five HH stage 11 hearts, corresponding to E1.5–E2 (*Materials and Methods*). Dashed lines indicate predicted E_0 values for the CE (blue) and SE (red) models, corresponding to the lower-stiffness cutoffs shown in Fig. 2*A*.

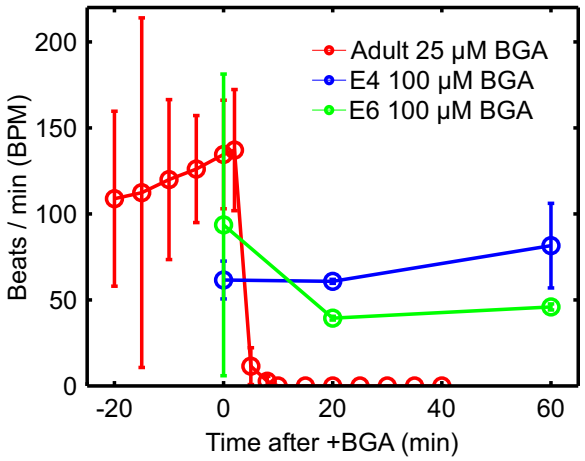

Fig. 4. Conduction interference results for isolated hearts from three murine adults and four chicken embryos. Gap junctions are disrupted by perfusing intact adult (red) and embryonic E4 and E6 (blue and green, respectively) hearts with β-glycyrrhetinic acid (BGA). Heart functionality is quantified by beats per minute (BPM). Adult hearts stop beating after ~10 min at 25 μM BGA (Movie S2). Embryonic hearts perfused at higher 100 μM show little to no effect after an hour. See Fig. S3 for adult heart BPM controls and Fig. S4 for control experiments on embryonic heart BGA perfusion.

contracts with a probability $p(\epsilon_{kk})$ that increases with strain, and found similar stiffness dependence of the contractile wave front. This stochastic activation model corresponds mathematically to stochastic pulse-coupled oscillator (SPCO) models of neural networks (35), but with an additional spatially dependent phase set by mechanical reaction–diffusion. Synchronized states in SPCO models map onto steady-state wave fronts of our stochastic model.

We note that embryonic CMs spontaneously contract in periodic manner (3, 4). In the beating embryonic heart, the wave front is initiated at the atrial end of the heart tube by CMs that contract at a higher frequency. Our model describes the nonlinear propagating wave front emanating from each contraction of these atrial CMs that activates other CMs. An alternate but equivalent description is to consider the coordination of CMs as nonlinear oscillators coupled through the ECM. Because the ECM has a viscous fluid component as well as an elastic component, this coupling does not lead to synchronization, as typical for phase-coupled biological oscillators (36), but to a propagating wave front.

Mechanical Signaling Is Consistent with Known Mechanosensitivity of CMs. There is solid evidence that stretch can trigger contraction of CMs. External tissue-scale stretch of the heart triggers arrhythmic beats (37). Healthy adult rat CMs exhibit increased intracellular calcium release events under 8% strain (38), whereas diseased adult myocytes demonstrate direct mechano-chemotransduction through full intracellular calcium release (9). Mechanical stimulation of the substrate in cultured embryonic chick CMs with 6% stretch excites quiescent myocytes (39). Mechanical stress exerted by fibroblasts affects the wave front velocity of neonatal rat CMs (40, 41), and neonatal and adult rat CMs cultured in similar conditions exhibit mechanical stimulation and entrainment (42). In some of these experiments, it is known that stretch-induced activation involves cardiac ryanodine receptors (9).

Mechanical vs. Electrical Signaling in the Developing Heart. There is evidence in the literature that electrical conduction may not be fully functional in the early heart. When whole-tissue contractions first appear, the cardiac conduction system is not yet identifiable (43). Embryonic chick hearts exhibit low levels of the primary cardiovascular gap junction protein, Connexin43 (Cx43), and the small amounts present are distributed uniformly through the cytosol until trabeculation occurs (44, 45). Other studies find that, in posthatch and adult chick, the primary ventricle myocardial gap junction is Cx42. However, Cx42 appears to be absent in working myocytes and cardiac conduction tissues until E9–E11, leading to speculation that CMs may not be electrically coupled by gap junctions during embryogenesis (46). Primary markers of the conduction system do not appear definitively until E9–E15 (47).

In conjunction with our results, such observations suggest that the heart may switch from mechanical to electrical signaling as it matures. We speculate that mechanically coordinated heartbeats may assist in organizing the heart: myocytes seeking to maximize contractile activity will align with each other (48) and cyclic stretch of neonatal rat ventricular myocytes was found to polarize gap junction localization (49). Perhaps current limitations in producing fully mature CMs from stem cells (15) reflect an incomplete understanding of the role of mechanics in heart development.

It is possible that mechanical signaling prevails in early development because it is robust. Electrical coupling requires gap junctions, which may be difficult to maintain as CMs proliferate and rearrange in the rapidly growing heart. Mechanical signals, on the other hand, are inevitably present because CMs must exert stresses on their surroundings when they contract. However, electrical signaling is easier to regulate when the heart develops more complicated structure.

In summary, the highly sophisticated electrical conduction system that precisely regulates the adult heart has been assumed to coordinate every heartbeat, from the first to the last. Here, we use a biophysical theory, bolstered by experiment, to propose that mechanical—not electrical—signaling is responsible for coordinating early heartbeats. If further verified, this idea could transform the way we think about how the heart develops and functions.

Materials and Methods

Model Details. We solve the matrix response function in three dimensions. We assume a stationary constant-velocity wave front $[\epsilon_{ij}(x, t) = \epsilon_{ij}(x - vt)]$ within a cubic array of infinitesimal active sites. The infinitesimal approximation was validated through finite element simulation (*Supporting Information* and Fig. S7). Self-consistency of the activation condition with the time between activation events relates v to model parameters. See *Supporting Information*.

Numerical Computations and Data Analysis. Numerical computations were performed in C/C++ and MATLAB. Data analysis and nonlinear least-squares parameter fitting was done in MATLAB with custom subroutines.

Finite-Element Simulation. Linear elastic finite-element simulations were performed in MATLAB and COMSOL. Cell-on-gel culture was modeled as a hemisphere adhered to a substrate. See *Supporting Information* and Table S1 for simulation parameters.

Myocardium Stiffness Measurements. Embryonic hearts were isolated as described in ref. 10. Aspiration was performed at room temperature. See *Supporting Information*.

Conduction Interference: Embryonic Hearts. Embryonic chick hearts were isolated as in ref. 10 and incubated in heart medium at 37 °C (α-MEM supplemented with 10% (vol/vol) FBS and 1% penn-strep; Gibco; 12571-063) for at least 2 h before drug treatment. Desired concentrations of 18-β-glycyrrhetinic acid (Cayman Chemical; 11845) and blebbistatin (EMD Millipore; 203390) were prepared by diluting in heart culture medium [with or without 10% (vol/vol) FBS] and DMSO, respectively. Isolated hearts were then treated with BGA or blebbistatin by aspirating out the medium and perfusing the hearts in the prepared drug solutions. E4 hearts were imaged using an Olympus I81 microscope and recorded for a minimum of 15 s using a CCD camera at 21 frames per s. E6 hearts were imaged using a Nikon SMZ1500 microscope. Analysis was performed in ImageJ by tracking morphological parameters over 10- to 15-s intervals.

Conduction Interference: Adult Hearts. Adult (8–12 wk) C57/BL6 mice were anesthetized by induction in an isoflurane chamber, followed by thoracotomy and excision of the heart. Isolated hearts were suspended from a Langendorff perfusion column via cannulation of the aorta and perfused with an oxygenated heart medium at 37 °C. Under control conditions, hearts cannulated via this method generate intrinsic rhythm and maintain rhythmic beating for over 3 h. BGA solution was prepared by dilution in medium and DMSO. After ensuring 20 min of rhythmic beating, the medium was exchanged for BGA-prepped solution. Twenty-second movie acquisitions were acquired every 3–5 min to analyze changes in heart rate over time. Experiments were terminated if the heart stopped beating for more than 10 min. Movie segments from different time points were randomized and analyzed blindly to determine beats per minute from 20-s intervals.

ACKNOWLEDGMENTS. We thank B. Davidson, T. Idema, S. Leibler, S. Safran, and J. Sethna for instructive discussions, and the Simons Center for Systems Biology at the Institute for Advanced Study for its hospitality (A.J.L.). We gratefully acknowledge support from Charles E. Kaufman Foundation Grant KA2015-79179 (to K.K.C., A.J.L., D.E.D., C.Y.C., and B.L.P.). In addition, the work was supported by the NSF through Grant DMR-1506625 (to K.K.C. and A.J.L.); the NIH through Grants U54-CA193417, R21-HL128187, and 8UL1TR000003 (to S.C., K.V., M.T., S.F.M., and D.E.D.), R00-HL114879 (to B.L.P.), and T32-AR053461 (to P.R.); and the AHA through Grant 14GRNT20490285 (to D.E.D.). J.W.R. was supported by an NSF graduate fellowship. This work was partially supported by a Simons Theoretical Fellowship (Grant 305547) and a Simons Investigator Award from the Simons Foundation (to A.J.L.), by the NSF-MRSEC (to A.J.L. and D.E.D.), and by the US/Israel Binational Science Foundation (to D.E.D.).

1. Keith A, Flack MW (1906) The auriculo-ventricular bundle of the human heart. *Lancet* 2(4328):359–364.
2. Kanno S, Saffitz JE (2001) The role of myocardial gap junctions in electrical conduction and arrhythmogenesis. *Cardiovasc Pathol* 10(4):169–177.
3. Sasse P, et al. (2007) Intracellular Ca^{2+} oscillations, a potential pacemaking mechanism in early embryonic heart cells. *J Gen Physiol* 130(2):133–144.
4. Rapila R, Korhonen T, Tavi P (2008) Excitation-contraction coupling of the mouse embryonic cardiomyocyte. *J Gen Physiol* 132(4):397–405.
5. Jacot JG, McCulloch AD, Omens JH (2008) Substrate stiffness affects the functional maturation of neonatal rat ventricular myocytes. *Biophys J* 95(7):3479–3487.
6. Engler AJ, et al. (2008) Embryonic cardiomyocytes beat best on a matrix with heart-like elasticity: Scar-like rigidity inhibits beating. *J Cell Sci* 121(Pt 22):3794–3802.
7. Bhana B, et al. (2010) Influence of substrate stiffness on the phenotype of heart cells. *Biotechnol Bioeng* 105(6):1148–1160.
8. Hersch N, et al. (2013) The constant beat: Cardiomyocytes adapt their forces by equal contraction upon environmental stiffening. *Biol Open* 2(3):351–361.
9. Prosser BL, Ward CW, Lederer WJ (2011) X-ROS signaling: Rapid mechano-chemo transduction in heart. *Science* 333(6048):1440–1445.
10. Majkut S, et al. (2013) Heart-specific stiffening in early embryos parallels matrix and myosin expression to optimize beating. *Curr Biol* 23(23):2434–2439.
11. Nash MP, Panfilov AV (2004) Electromechanical model of excitable tissue to study reentrant cardiac arrhythmias. *Prog Biophys Mol Biol* 85(2-3):501–522.
12. Panfilov AV, Keldermann RH, Nash MP (2007) Drift and breakup of spiral waves in reaction-diffusion-mechanics systems. *Proc Natl Acad Sci USA* 104(19):7922–7926.
13. Idema T, Liu AJ (2014) Mechanical signaling via nonlinear wavefront propagation in a mechanically excitable medium. *Phys Rev E Stat Nonlin Soft Matter Phys* 89(6):062709.
14. Dawson SP, Keizer J, Pearson JE (1999) Fire-diffuse-fire model of dynamics of intracellular calcium waves. *Proc Natl Acad Sci USA* 96(11):6060–6063.
15. Burridge PW, Keller G, Gold JD, Wu JC (2012) Production of de novo cardiomyocytes: Human pluripotent stem cell differentiation and direct reprogramming. *Cell Stem Cell* 10(1):16–28.
16. Vogel V, Sheetz M (2006) Local force and geometry sensing regulate cell functions. *Nat Rev Mol Cell Biol* 7(4):265–275.
17. Wozniak MA, Chen CS (2009) Mechanotransduction in development: A growing role for contractility. *Nat Rev Mol Cell Biol* 10(1):34–43.
18. Wang N, Tytell JD, Ingber DE (2009) Mechanotransduction at a distance: Mechanically coupling the extracellular matrix with the nucleus. *Nat Rev Mol Cell Biol* 10(1):75–82.
19. DuFort CC, Paszek MJ, Weaver VM (2011) Balancing forces: Architectural control of mechanotransduction. *Nat Rev Mol Cell Biol* 12(5):308–319.
20. Shaw J, Izu L, Chen-Izu Y (2013) Mechanical analysis of single myocyte contraction in a 3-D elastic matrix. *PLoS One* 8(10):e75492.
21. McCain ML, Lee H, Aratyn-Schaus Y, Kléber AG, Parker KK (2012) Cooperative coupling of cell-matrix and cell-cell adhesions in cardiac muscle. *Proc Natl Acad Sci USA* 109(25):9881–9886.
22. Hazeltine LB, et al. (2012) Effects of substrate mechanics on contractility of cardiomyocytes generated from human pluripotent stem cells. *Int J Cell Biol* 2012: 508294.
23. Dasbiswas K, Majkut S, Discher DE, Safran SA (2015) Substrate stiffness-modulated registry phase correlations in cardiomyocytes map structural order to coherent beating. *Nat Commun* 6:6085.
24. Mura T (1987) Isotropic inclusions. *Micromechanics of Defects in Solids* (Springer, Dordrecht, The Netherlands), pp 74–128.
25. Phillips R (2001) Inclusions as microstructure. *Crystals, Defects, and Microstructures* (Cambridge Univ Press, Cambridge, UK), pp 520–546.
26. Hu Z, Metaxas D, Axel L (2003) In vivo strain and stress estimation of the heart left and right ventricles from MRI images. *Med Image Anal* 7(4):435–444.
27. Mow VC, Kuei SC, Lai WM, Armstrong CG (1980) Biphasic creep and stress relaxation of articular cartilage in compression? Theory and experiments. *J Biomech Eng* 102(1): 73–84.
28. Banerjee S, Marchetti MC (2001) Instabilities and oscillations in isotropic active gels. *Soft Matter* 7(2):463–473.
29. Guevorkian K, Gonzalez-Rodriguez D, Carlier C, Dufour S, Brochard-Wyart F (2011) Mechanosensitive shivering of model tissues under controlled aspiration. *Proc Natl Acad Sci USA* 108(33):13387–13392.
30. Le AC, Musil LS (1998) Normal differentiation of cultured lens cells after inhibition of gap junction-mediated intercellular communication. *Dev Biol* 204(1):80–96.
31. Böhmer C, Kirschner U, Wehner F (2001) 18-beta-Glycyrrhetinic acid (BGA) as an electrical uncoupler for intracellular recordings in confluent monolayer cultures. *Pflugers Arch* 442(5):688–692.
32. Sato T, Nishishita K, Okada Y, Toda K (2009) Effect of gap junction blocker beta-glycyrrhetinic acid on taste disk cells in frog. *Cell Mol Neurobiol* 29(4):503–512.
33. Xia Y, Nawy S (2003) The gap junction blockers carbenoxolone and 18beta-glycyrrhetinic acid antagonize cone-driven light responses in the mouse retina. *Vis Neurosci* 20(4):429–435.
34. Davidson JS, Baumgarten IM, Harley EH (1986) Reversible inhibition of intercellular junctional communication by glycyrrhetinic acid. *Biochem Biophys Res Commun* 134(1):29–36.
35. DeVille REL, Peskin CS (2008) Synchrony and asynchrony in a fully stochastic neural network. *Bull Math Biol* 70(6):1608–1633.
36. Mirollo RE, Strogatz SH (1990) Synchronization of pulse-coupled biological oscillators. *SIAM J Appl Math* 50(6):1645–1662.
37. Stacy GP, Jr, Jobe RL, Taylor LK, Hansen DE (1992) Stretch-induced depolarizations as a trigger of arrhythmias in isolated canine left ventricles. *Am J Physiol* 263(2 Pt 2): H613–H621.
38. Iribe G, et al. (2009) Axial stretch of rat single ventricular cardiomyocytes causes an acute and transient increase in Ca^{2+} spark rate. *Circ Res* 104(6):787–795.
39. Tang X, Bajaj P, Bashir R, Saif TA (2011) How far cardiac cells can see each other mechanically. *Soft Matter* 7(13):6151–6158.
40. Thompson SA, Copeland CR, Reich DH, Tung L (2011) Mechanical coupling between myofibroblasts and cardiomyocytes slows electric conduction in fibrotic cell monolayers. *Circulation* 123(19):2083–2093.
41. Thompson SA, et al. (2014) Acute slowing of cardiac conduction in response to myofibroblast coupling to cardiomyocytes through N-cadherin. *J Mol Cell Cardiol* 68: 29–37.
42. Nitsan I, Drori S, Lewis YE, Cohen S, Tzlil S (2016) Mechanical communication in cardiac cell synchronized beating. *Nat Phys* 12:472–477.
43. Mikawa T, Hurtado R (2007) Development of the cardiac conduction system. *Semin Cell Dev Biol* 18(1):90–100.
44. Dealy CN, Beyer EC, Kosher RA (1994) Expression patterns of mRNAs for the gap junction proteins connexin43 and connexin42 suggest their involvement in chick limb morphogenesis and specification of the arterial vasculature. *Dev Dyn* 199(2):156–167.
45. Wiens D, Jensen L, Jasper J, Becker J (1995) Developmental expression of connexins in the chick embryo myocardium and other tissues. *Anat Rec* 241(4):541–553.
46. Gourdie RG, Green CR, Severs NJ, Anderson RH, Thompson RP (1993) Evidence for a distinct gap-junctional phenotype in ventricular conduction tissues of the developing and mature avian heart. *Circ Res* 72(2):278–289.
47. Gourdie RG, Kubalak S, Mikawa T (1999) Conducting the embryonic heart: Orchestrating development of specialized cardiac tissues. *Trends Cardiovasc Med* 9(1-2): 18–26.
48. Bischofs IB, Schwarz US (2003) Cell organization in soft media due to active mechanosensing. *Proc Natl Acad Sci USA* 100(16):9274–9279.
49. Salameh A, et al. (2010) Cyclic mechanical stretch induces cardiomyocyte orientation and polarization of the gap junction protein connexin43. *Circ Res* 106(10):1592–1602.
50. Vinnakota KC, Bassingthwaighte JB (2004) Myocardial density and composition: A basis for calculating intracellular metabolite concentrations. *Am J Physiol Heart Circ Physiol* 286(5):H1742–H1749.
51. von Zglinicki T, Bimmler M (1987) The intracellular distribution of ions and water in rat liver and heart muscle. *J Microsc* 146(Pt 1):77–85.